

Floquet-engineered vibrational dynamics in a two-dimensional array of trapped ions

Philip Kiefer,^{1,*} Frederick Hakeberg,¹ Matthias Wittemer,¹
Alejandro Bermúdez,^{2,†} Diego Porras,^{3,‡} Ulrich Warring,¹ and Tobias Schaetz¹

¹*Albert-Ludwigs-Universität Freiburg, Physikalisches Institut,
Hermann-Herder-Strasse 3, 79104 Freiburg, Germany*

²*Departamento de Física Teórica, Universidad Complutense, 28040 Madrid, Spain*

³*Instituto de Física Fundamental IFF-CSIC, Calle Serrano 113b, 28006 Madrid, Spain*

(Dated: July 16, 2019)

We demonstrate Floquet engineering in a basic yet scalable 2D architecture of individually trapped and controlled ions. Local parametric modulations of detuned trapping potentials steer the strength of long-range inter-ion couplings and the related Peierls phase of the motional state. In our proof-of-principle, we initialize large coherent states and tune modulation parameters to control trajectories, directions and interferences of the phonon flow. Our findings open a new pathway for future Floquet-based trapped-ion quantum simulators targeting correlated topological phenomena and dynamical gauge fields.

A promising route for the exploration of complex quantum dynamics is to use experimental simulator devices where synthetic interactions and quantum states can be efficiently controlled [1]. In general, systems of interest should provide long-range interactions and spatial dimensions higher than one since these remain beyond the reach of numerical methods [2]. A variety of prototype platforms already exists [3]. Trapped atomic ions are a promising approach, featuring identical constituents, long range Coulomb forces, and unique control of internal (electronic) and external (phonon) degrees of freedom [4, 5]. Tremendous progress in common trapping potentials has been achieved [6, 7]. Furthermore experiments have shown coupling of individual ions at distant sites by matching local motional frequencies in 1D [8–10] and in scalable 2D arrangements [11] with the perspective to preserve the unique control of one/few ion ensembles. Typically, quantized vibrations (phonons) are used as an auxiliary bus mediating entangling gate operations [12], or synthetic spin-spin interactions [13]. In contrast, it has been proposed to actively use this degree of freedom. For example, to simulate complex bosonic lattice models [14] and to Floquet engineer an effective Peierls phase of the motional state, analogous to a synthetic gauge field [15, 16]. In this context, phonons, represent charged particles in external electromagnetic fields. They tunnel, their trajectories enclose areas related to geometric phases or interfere directly between individually controlled ions, located at distinct sites of a dedicated lattice structure. A realization requires fine tuning and parametric modulations of motional frequencies at each site. The strength of these drives tune the tunneling (coupling) strength, while control of the relative phases controls the accumulated Peierls phase. Such modulations enable inter-ion couplings between detuned (decoupled) trapping potentials by absorption and emission of energy (photons or phonons) out of the classical driving field. Certain aspects of Floquet engineering by periodic modulations [17] have already been demonstrated for ultra-cold

atoms [18–20], superconducting qubits [21], and photonic lattices [22].

In this Letter, we show essential features of phonon assisted coupling of individual atomic ions trapped at micro sites of our triangular two-dimensional trap array. Parametric drives applied to single or multiple locations steer constructive and destructive coherent couplings within the array. Tuning driving amplitudes and relative phases, we control directionality and interference of the phonon flow via the related synthetic Peierls phase of the motional states, a key requirement for future quantum Floquet engineering.

We trap magnesium ions in our surface-electrode trap array featuring separate micro sites $T_{\mathbf{j}}$, where $\mathbf{j} \in \{0, 1, 2\}$ labels the corners of the triangle with side lengths of $40 \mu\text{m}$ and an ion-surface distance of $\simeq 40 \mu\text{m}$ [23, 24]. In harmonic approximation, these distances yield an inter-site coupling strength $\Omega_C/(2\pi) \simeq 1 \text{ kHz}$ for motional frequencies $\omega_{\mathbf{j}}/(2\pi) \simeq 4 \text{ MHz}$. Heating rates of (1–10) quanta/ms are derived from calibration measurements close to the motional ground state [25, 26]. In order to receive unambiguous signals of the phonon dynamics we initialize coherent states (exceeding $\simeq 1,000$ motional quanta). The effective coupling rate $\Omega_{C,\text{eff}}$ is tunable via relative motional mode orientations and the detuning of the individual trapping sites. Anharmonic contributions of the trapping potential lead to an increased $\Omega_{C,\text{eff}}/(2\pi) \simeq 6 \text{ kHz}$, while the related efficiency is reduced accordingly [11]. Quasi-static control potentials locally tune electric fields, curvatures and higher order terms, e.g. for preparation/detection or inter-site couplings [11]. We adiabatically ramp these control potentials within $t_{\text{ramp}} \leq 100 \mu\text{s}$ ($t_{\text{ramp}} \geq (\omega_{\mathbf{j}})^{-1}$) between different configurations. Additionally, we can apply various local periodic control potentials $\phi_{\mathbf{j}}^{\text{osc}}(\Omega_{\mathbf{j}}^{\text{osc}}, \varphi_{\mathbf{j}}^{\text{osc}}, u_{\mathbf{j}}^{\text{osc}})$ for duration $t_{\mathbf{j}}^{\text{osc}}$, oscillating with frequency $\Omega_{\mathbf{j}}^{\text{osc}}$ with a tunable phase $\varphi_{\mathbf{j}}^{\text{osc}}$ and amplitude $u_{\mathbf{j}}^{\text{osc}}$, allowing for: (i) Floquet engineering by a parametric modulation $\phi_{\mathbf{j}}^M$ of

motional frequencies with $\Omega_j^M/(2\pi) \simeq 100$ kHz or (ii) Initialization of a vibronic coherent state at a given T_j by a local excitation via ϕ_j^ξ . All experiments are initialized by global Doppler cooling, aligning the local mode orientations, and tuning the lowest motional frequencies to $\omega_j/(2\pi) \simeq (3-5)$ MHz [11, 23]. In following steps (see below) we apply dedicated control potentials for individual settings, and finish by local fluorescence detection allowing to derive average phonon numbers \bar{n}_j . The reduction of the fluorescence rate allows us to derive the increase of \bar{n}_j . Each sequence is repeated 200 to 400 times to derive the standard error of the mean (s.e.m.).

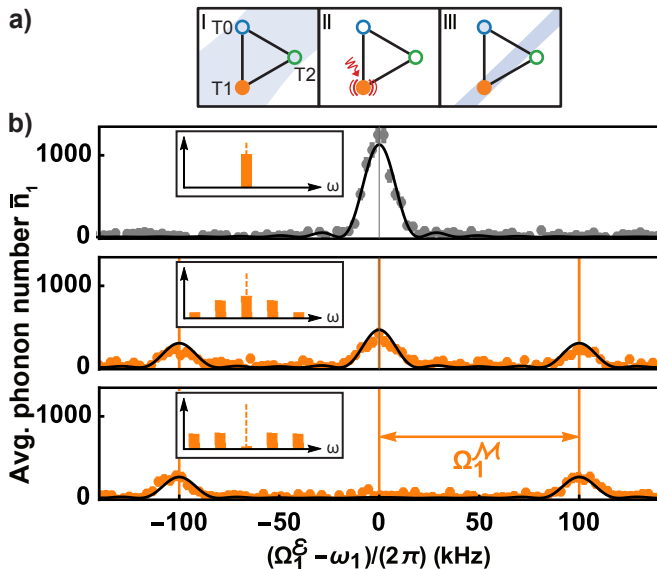


FIG. 1. **Characterization of the ion's frequency spectrum during modulation at a single site.** a) Experimental sequence to characterize the effect of the modulation at T_1 on the motional eigenfrequency ω_1 and its sidebands. These sidebands are interpreted as channels that in case of spectral overlap can permit transmission between neighboring T_j . The three, equidistant trapping sites are marked by colored circles, the presence of an ion by a disk. (I) A single ion at T_1 is prepared via laser cooling (shaded area). (II) The effect of the modulation potential ϕ_1^M with variable strength (red brackets) is probed simultaneously via the excitation field $\phi_1^\xi(\Omega_1^\xi)$ (red wiggled arrow) for duration $t_1^\xi = t_1^M = 50$ μ s. (III) Local detection of fluorescence from T_1 enables reconstruction of the ion's motional amplitude. (b) Final motional amplitudes (data points, errorbars s.e.m.) in dependence on excitation frequency Ω_1^ξ : (top) no modulation and (middle, bottom) increasing modulation amplitude. Model fits to the data (solid lines, see [24]) allow to calibrate the reference coherent excitation, i.e. $\eta_1 = 0$ (top) and modulation indices with statistic uncertainties $\eta_1 = 1.26(3)$, $2.57(4)$ (middle, bottom). Bar charts (insets) illustrate the derived amplitudes for the equally spaced spectral channels, shown up to the second sidebands. In this way, we can, e.g., strongly suppress excitations at the local oscillator frequency ω_1 (b, bottom).

To calibrate Floquet engineering via oscillating potentials ϕ_j^M , see [24], we perform measurements with single

ions at T_j . Exemplarily, we discuss results for site T_1 , see Fig. 1, where we probe the effect of $\phi_1^M(\Omega_1^M, u_1^M)$ for fixed $\Omega_1^M/(2\pi) = 100$ kHz $\ll \omega_1/(2\pi)$ with a simultaneously applied drive for coherent excitation $\phi_1^\xi(\Omega_1^\xi, u_1^\xi)$. Tuning Ω_1^ξ across ω_1 , we show reconstructed motional amplitudes for $u_1^M = 0$ V (top), 150 mV (middle), and 250 mV (bottom) in dependence on Ω_1^ξ . When ϕ_1^M is switched on, a comb structure is spanned by several channels (sidebands) at $\Omega_1^\xi \simeq \omega_1 + m\Omega_1^M$ with $m \in \mathbb{Z}$. Floquet theory (solid lines) predicts that the relative strength of these channels is defined by the m -th order Bessel function of the first kind $\mathcal{J}_m(\eta_j)$, where $\eta_j \propto u_j^M/\Omega_j^M$ represents the modulation index [24]. For increasing u_1^M (Fig. 1(b) middle, bottom), the carrier channel decreases, until $\mathcal{J}_0(\eta_j)$ crosses zero. This channel gets effectively shut and can lead in following experiments where we couple neighboring sites to so-called coherent destruction of tunneling [27]. Overall, we find $\eta_j\Omega_j^M/(2\pi)$ of up to 300 kHz for $\Omega_j^M/(2\pi) \simeq (50 - 200)$ kHz.

To demonstrate control of synthetic Peierls phases imprinted on the motional state in real-time, we explore the assisted transfer of energy, i.e. flow of phonons, between ions at different T_j . As an example we perform our experiment with single ions at T_0 and T_1 , see Fig. 2. We adjust the inter-site detuning to $\Delta\omega_{01}/(2\pi) = (\omega_1 - \omega_0)/(2\pi) \simeq 100$ kHz, and excited the ion at T_0 (ϕ_0^ξ for $t_0^\xi = 20$ μ s) to $\bar{n}_0 = (5,000 - 10,000)$. By choice of $\Delta\omega_{01}$ the coupling efficiency (for $\eta_j = 0$) is suppressed by four orders of magnitude. Setting $\Omega_1^M = \Delta\omega_{01}$, $\eta_1 \simeq 1.8$, at a fixed φ_1^M , the phonon exchange is enabled by assistance of ϕ_1^M : a single transmission channel is opened by overlapping the lower first sideband at T_1 with the carrier at ω_0 of T_0 , see Fig. 2(b, inset). In Figure 2(b), we show reconstructed \bar{n}_1 as a function of t_1^M . We model the coherent exchange, absorption and emission, of phonons, with corresponding assisted coupling rate Ω_{AC} (solid line, see [24]). We thus confirm that the ion at T_1 absorbs up to $\simeq 820$ phonons after $t_\pi = \pi/\Omega_{AC}$. The efficiency is limited to about 15% of \bar{n}_0 . We attribute that to the anharmonicity of the trapping potential probed by the currently large \bar{n}_1 [11]. The anharmonic effects can be interpreted as additional detuning, increasing Ω_{AC} but limiting efficiency.

The Peierls phase $\Phi^P(t)$ plays an important role in the Floquet engineered Hamiltonian of energy transfer between different sites [24]. It is given by the path integral along l between trapping sites $\Phi^P(t) = \frac{q}{\hbar} \int_{T_0}^{T_1} dl \cdot \mathbf{A}(\mathbf{r}, t)$, where \hbar is the reduced Planck constant. Φ^P rules the dynamics of the phonons as if they were particles with charge q coupled to a gauge potential $\mathbf{A}(\mathbf{r}, t)$. In an extended experimental sequence the evolution of Φ^P is controlled in real-time during the experiment. In particular, after a period of assisted coupling of $t_{1,\text{prep}}^M = t_\pi/2 \simeq 150$ μ s, we adiabatically ramp $\varphi_1^M \rightarrow \varphi_1^M + \Delta\varphi_1^M$ within $t_{\varphi,\text{ramp}} = 25$ μ s $\gg \omega_j^{-1}$, and continue the modulation for duration $t_1^M - (t_{1,\text{prep}}^M + t_{\varphi,\text{ramp}})$. We depict normalized

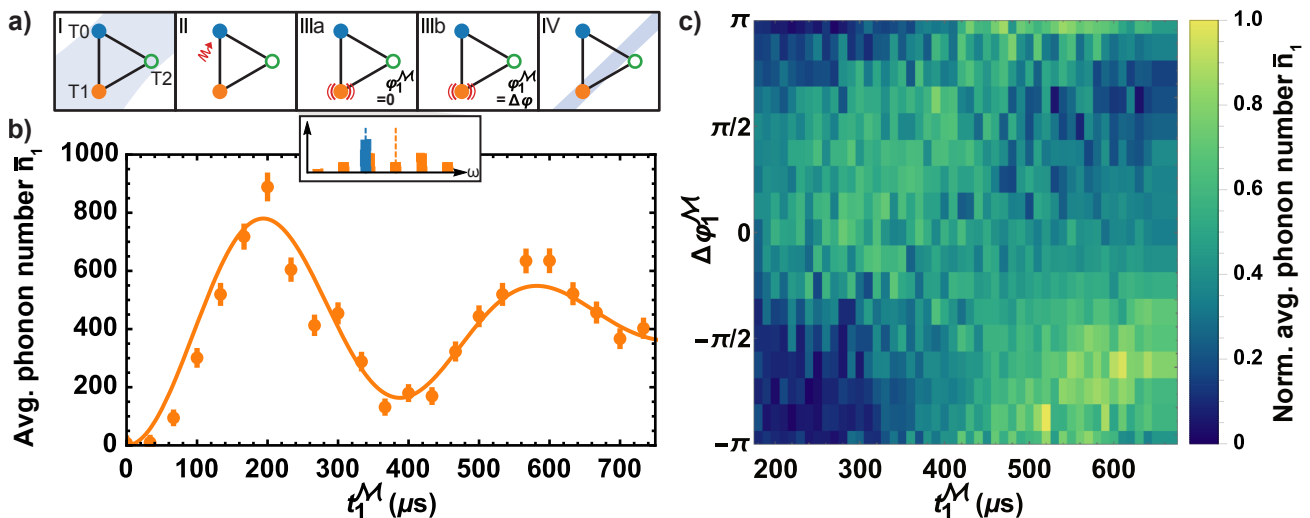


FIG. 2. **Inter-site coupling assisted by single-site modulation, enabling the control of directionality of the phonon flow.** (a) Experimental sequence: (I) Initializing single ions at T_0 and T_1 . (II) Switching to detuned coupling configuration and excite the ion at T_0 . (IIIa) Launching inter-site coupling by application of ϕ_1^M . (IIIb) To optionally redirect the phonon flow after 150 μs , we change the phase of ϕ_1^M . Here $\Delta\varphi_1^M$ is realized within 25 μs , while ϕ_1^M is active in total for t_1^M . (IV) Detecting the motional amplitude \bar{n}_1 . (b) Motional amplitude at T_1 as a function of t_1^M (data points, errorbars s.e.m.) using part (IIIa). We choose ϕ_1^M to open efficiently the transmission channel of the first lower sideband at T_1 (inset, orange bar chart) and the carrier at T_0 (blue bar, slightly shifted for visibility). Phonons are coherently exchanged between T_0 and T_1 . A model fit (solid line) yields an assisted coupling rate $\Omega_{AC}/(2\pi) = 2.51(5)$ kHz and dephasing duration of $\tau = 550(60)$ μs . (c) Normalized motional amplitude in dependence on t_1^M and $\Delta\varphi_1^M$ including sequence part (IIIb). Real-time control of the Peierls phase $\Phi^P(t)$ and the related directionality of the phonon flow is set by $\Delta\varphi_1^M$.

\bar{n}_1 as a function of $\Delta\varphi_1^M$ and t_1^M in Fig. 2(c). The dependence of the number of exchanged phonons on $\Delta\varphi_1^M$ shows that Φ^P cannot be simply gauged away for $\Delta\varphi_1^M \neq 0$ but, instead, it serves to control the directionality of the coherent energy flow. At $t_1^M \simeq 300$ μs , optimal exchange is observed for $\Delta\varphi_1^M \simeq +\pi/4$. For $\Delta\varphi_1^M \approx -3\pi/4$, a change by π , we observe the transferred population nearly vanishing. This is consistent with Floquet theory, which predicts that $\Omega_{AC}(\varphi_1^M) \rightarrow -\Omega_{AC}(\varphi_1^M + \pi)$, equivalent to a time-reversal operation. That is, it returns phonons from T_1 back to T_0 and further simulates the application of an electric field on charged particles. In particular, $\partial\Phi^P(t)/\partial t \neq 0$ can be understood as a background synthetic electric field $\mathbf{E}(\mathbf{r}, t) = -\partial\mathbf{A}(\mathbf{r}, t)/\partial t$. We observe a global shift by $\pi/4$ in the data. Numerical simulations can provide evidence for a similar shift, when considering a mismatch between Ω_1^M and $\Delta\omega_{01}$ of a few percent and the finite ramping duration $t_{\varphi, \text{ramp}}$.

In the next sequence, we explore the dynamics between T_0 and T_1 when both sites are locally driven by ϕ_0^M and ϕ_1^M at fixed $\Omega_0^M = \Omega_1^M \simeq \Delta\omega_{01}$ and $\eta_0 \simeq \eta_1$. In this case, the assisted exchange can be controlled by the relative modulation phase $\Delta\varphi_{01}^M = \varphi_0^M - \varphi_1^M$, here reaching $\Omega_{AC}/(2\pi) \leq 4.5$ kHz [11]. As shown in Fig. 3(b, c inset), we open several transmission channels, and the overall phonon exchange is governed by constructive or destructive interference of all contributions as a function of $\Delta\varphi_{01}^M$. We show results of \bar{n}_1 after $t_{01}^M \simeq t_\pi$

for $\eta_0 \simeq \eta_1 \simeq \eta \simeq \{0.9, 1.7\}$ in Figs. 3(b) and (c), respectively. For $\eta \simeq 0.9$, transmission is predominantly enabled by the resonance of two distinct channels, corresponding to the carriers and first sidebands at T_0 and T_1 , cf. Fig. 3(b, inset). As shown in Fig. 3(b), the measured data is consistent with the Floquet-engineered Ω_{AC} , considering a linear coupling between harmonic oscillators (dashed line) [16]: Ω_{AC} and the transfer to T_1 is maximal and robust around $\Delta\varphi_{01}^M = \pi$, while it is significantly suppressed for $\Delta\varphi_{01}^M = 0$ and 2π . A residual coupling for these values can be explained by a residual mismatch of the modulation indices ($\eta_0 \neq \eta_1$) and inter-site dephasing. Stronger modulation, see Fig. 3(c, inset) opens additional channels, i.e., leads to larger contribution of upper and lower sidebands. In Figure 3(c) data shows additional features of phase dependent energy transfer, e.g. an additional destructive interference near $\Delta\varphi_{01}^M = \pi$ in accordance with the prediction. We note, however, that the two peaks of maximal phonon exchange are narrowed with respect to the idealized theory, and a slight asymmetry appears, which we attribute to anharmonicities resulting from the Coulomb interaction, as well as local trapping potentials.

To demonstrate interference of phonons in two dimensions, akin to the Aharonov-Bohm effect of charged particles under an external magnetic field, all T_j are initialized. We prepare for multi-site coupling by tuning $\omega_{\{0,1,2\}}/(2\pi) \simeq \{4.9, 5.0, 5.1\}$ MHz. We simulta-

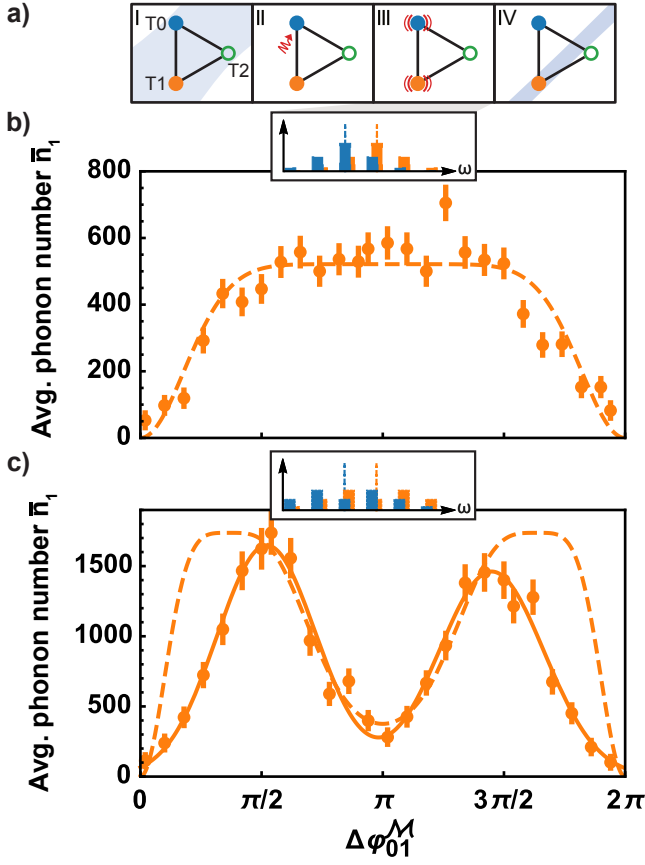


FIG. 3. **Tunable assisted coupling, established by selection of transmission channels and its dependence on the relative phase of two modulations.** (a) Experimental sequence: (I) Preparation of single ions at T_0 and T_1 . (II) Initialization of phonons at T_0 by application of ϕ_0^ε at detuned inter-site coupling configuration. (III) Activation of assisted coupling by ϕ_0^M and $\phi_1^M(\Delta\varphi_{01}^M)$ with $\eta \simeq \eta_0 \simeq \eta_1$ for $t^M = t_\pi$, i.e. optimized exchange. (IV) Detection at T_1 . (b, c) Motional amplitude (data points, errorbars s.e.m.) in dependence on $\Delta\varphi_{01}^M$ for (b) $\eta \simeq 0.9$ and (c) $\eta \simeq 1.7$. (Insets) Illustration of multiple transmission channels that mutually interfere and provide the effective coupling. The idealized, scaled model (dashed lines) describes the dependency qualitatively well, while it lacks to explain systematics in (c) outside the central region (guide to the eye: solid line), see text. Fundamentally, the energy transfer is a consequence of interferences of all transmission channels and is tuned by $\Delta\varphi_{01}^M$ at $\eta_0 \simeq \eta_1$.

neously apply $\phi_0^\varepsilon(\varphi_0^\varepsilon)$ and $\phi_2^\varepsilon(\varphi_2^\varepsilon)$, to prepare coherent states with $\bar{n}_0 \simeq 5500$ and $\bar{n}_2 \simeq 5800$ phonons and, importantly, a fixed phase relation $\Delta\varphi_{02}^\varepsilon$ [28]. Multi-site phonon coupling is activated by applying ϕ_1^M with $\Omega_1^M \simeq \Delta\omega_{01} \simeq \Delta\omega_{12}$ and $\eta_1 \simeq 1.8$ during t_1^M . The lower and upper first sideband at T_1 opens transmission channels with the carrier at site T_0 and T_2 , respectively, see Fig. 4(b, top). We note that direct phonon exchange between T_0 and T_2 is disabled by the frequency mismatch $\Delta\omega_{02} \gg \Omega_{AC}$. Results in Fig. 4(b) depict \bar{n}_1 as

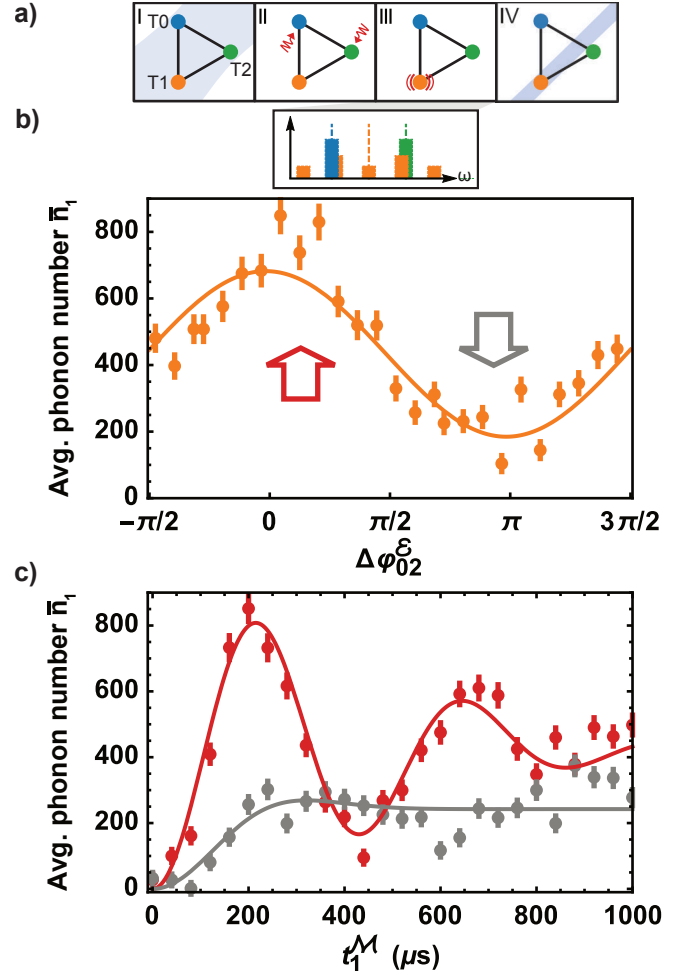


FIG. 4. **Controlled interference within a modulation-assisted 2D network of coupled oscillators.** (a) Experimental sequence: (I) Global preparation of single ions at T_j . (II) Coupled network configuration offers a local gradient between the individual trapping sites $\Delta\omega_{01} = \Delta\omega_{12}$. Two local excitation pulses control the relative phase between coherent states at T_0 and T_2 . (III) Coupling the network via modulation ϕ_1^M for t_1^M . (IV) Detection at T_1 . (b, top) Modulation ϕ_1^M opens transmission channels between T_0 and T_1 as well as between T_1 and T_2 . (b, bottom) Average phonon number \bar{n}_1 as a function of $\Delta\varphi_{02}^\varepsilon$ for $t_1^M = 200 \mu\text{s}$ (data points, errorbars s.e.m.). The orange line represents a sinusoidal model fit yielding an amplitude of 250(20) quanta and an offset of 430(20) quanta. (c) Evolution for characteristic constructive (red) and destructive (gray) interference within the network. Model fits (solid lines) depict suppressed Ω_{AC} in the destructive case and dephasing durations of 620(50) μs (red) and 250(80) μs (gray). Phase dependent dephasing durations as well as residual oscillations in the destructive case will be further investigated.

a function of $\Delta\varphi_{02}^\varepsilon$ for the maximal exchange achieved at $t_1^M = t_\pi$. While the energy transfer is maximal at $\Delta\varphi_{02}^\varepsilon = 0$ (constructive interference highlighted by red arrow), it is minimal at $\Delta\varphi_{02}^\varepsilon = \pi$ (destructive interference highlighted by gray arrow). In Figure 4(c), we in-

investigate both of the extremal settings in dependence on t_1^M , depicting the coherent destruction of energy transfer in 2D.

To summarize, we demonstrate Floquet engineering of vibrational excitations in a 2D ion-trap array, present clear signatures of interference effects, and discuss the role of the arising dynamical Peierls phase. In future studies, argon-ion bombardment[29] or cryogenic environments[30] can reduce heating rates by more than two orders of magnitude permitting operation near the motional ground state for durations $\gg 1/\Omega_{AC}$, as established for short time scales already [25]. Furthermore triangular lattices, plaquettes to concatenate rhombic ladders and even more complex, non-periodic structures can be realized in future arrays [31, 32]. Combining these techniques with the presented Floquet toolbox may additionally enable to study the interplay of non-linearities, i.e. effective on-site phonon-phonon interaction, with the synthetic gauge fields. This would enable to explore correlated, symmetry-protected topological phases of bosons [33]. By exploiting laser cooling and heating mechanisms [34], we can build a phononic analog of photonic lattices [35–38] with a rich interplay between topological and dissipative effects. Application of state-dependent optical potentials, may further extend the quantum-simulation prospects of our platform by enabling state dependent transmission. In particular, by coupling the internal degrees of freedom to the vibrations, one may study bosonic lattice models in the presence of dynamical gauge fields, e.g. famous Aharonov-Bohm physics, cages and edge states [16, 39].

We thank J.-P. Schröder for help with the experimental control system. The trap chip was designed in collaboration with R. Schmied in a cooperation with the NIST ion storage group and produced by Sandia National Laboratories. This work was supported by the Deutsche Forschungsgemeinschaft (DFG) [SCHA 973/6-3]. P.K. and F.H. contributed equally to this work.

* philip.kiefer@physik.uni-freiburg.de;
https://www.qsim.uni-freiburg.de

† albermud@fucm.es

‡ d.porras@iff.csic.es

- [1] J. I. Cirac and P. Zoller, *Nat. Phys.* **8**, 264 (2012).
- [2] F. Verstraete, J. I. Cirac, and V. Murg, *Advances in Physics* **57**, 143 (2008).
- [3] I. M. Georgescu, S. Ashhab, and F. Nori, *Reviews of Modern Physics* **86**, 153 (2014).
- [4] C. J. Ballance, T. P. Harty, N. M. Linke, M. A. Sepiol, and D. M. Lucas, *Physical Review Letters* **117**, 060504 (2016).
- [5] J. P. Gaebler, T. R. Tan, Y. Lin, Y. Wan, R. Bowler, A. C. Keith, S. Glancy, K. Coakley, E. Knill, D. Leibfried, and D. J. Wineland, *Physical Review Letters* **117**, 060505 (2016).
- [6] J. Zhang, G. Pagano, P. W. Hess, A. Kyprianidis, P. Becker, H. Kaplan, A. V. Gorshkov, Z.-X. Gong, and C. Monroe, *Nature* **551**, 601 (2017).
- [7] E. Jordan, K. A. Gilmore, A. Shankar, A. Safavi-Naini, J. G. Bohnet, M. J. Holland, and J. J. Bollinger, *Physical Review Letters* **122**, 053603 (2019).
- [8] K. R. Brown, C. Ospelkaus, Y. Colombe, A. C. Wilson, D. Leibfried, and D. J. Wineland, *Nature* **471**, 196 (2011).
- [9] M. Harlander, R. Lechner, M. Brownnutt, R. Blatt, and W. Hänsel, *Nature* **471**, 200 (2011).
- [10] A. C. Wilson, Y. Colombe, K. R. Brown, E. Knill, D. Leibfried, and D. J. Wineland, *Nature* **512**, 57 (2014).
- [11] F. Hakelberg, P. Kiefer, M. Wittemer, U. Warring, and T. Schaetz, arXiv:1812.08552 (2018).
- [12] V. M. Schäfer, C. J. Ballance, K. Thirumalai, L. J. Stephenson, T. G. Ballance, A. M. Steane, and D. M. Lucas, *Nature* **555**, 75 (2018).
- [13] H. Schmitz, A. Friedenauer, C. Schneider, R. Matjeschik, M. Enderlein, T. Huber, J. Glueckert, D. Porras, and T. Schaetz, *Applied Physics B* **95**, 195 (2009).
- [14] D. Porras and J. I. Cirac, *Phys. Rev. Lett.* **92**, 207901 (2004).
- [15] A. Bermudez, T. Schaetz, and D. Porras, *Physical Review Letters* **107**, 150501 (2011).
- [16] A. Bermudez, T. Schaetz, and D. Porras, *New Journal of Physics* **14**, 053049 (2012).
- [17] A. Eckardt, *Reviews of Modern Physics* **89**, 011004 (2017).
- [18] M. Aidelsburger, M. Atala, S. Nascimbène, S. Trotzky, Y.-A. Chen, and I. Bloch, *Physical Review Letters* **107**, 255301 (2011).
- [19] J. Struck, C. Ölschläger, M. Weinberg, P. Hauke, J. Simonet, A. Eckardt, M. Lewenstein, K. Sengstock, and P. Windpassinger, *Physical Review Letters* **108**, 225304 (2012).
- [20] L. Asteria, D. T. Tran, T. Ozawa, M. Tarnowski, B. S. Rem, N. Fläschner, K. Sengstock, N. Goldman, and C. Weitenberg, *Nature Physics* **15**, 449 (2019).
- [21] P. Roushan, C. Neill, A. Megrant, Y. Chen, R. Babush, R. Barends, B. Campbell, Z. Chen, B. Chiaro, A. Dunsworth, A. Fowler, E. Jeffrey, J. Kelly, E. Lucero, J. Mutus, P. J. J. O’Malley, M. Neeley, C. Quintana, D. Sank, A. Vainsencher, J. Wenner, T. White, E. Kapit, H. Neven, and J. Martinis, *Nature Physics* **13**, 146 (2017).
- [22] S. Mukherjee, M. Di Liberto, P. Öhberg, R. R. Thomson, and N. Goldman, *Physical Review Letters* **121**, 075502 (2018).
- [23] M. Mielenz, H. Kalis, M. Wittemer, F. Hakelberg, U. Warring, R. Schmied, M. Blain, P. Maunz, D. L. Moehring, D. Leibfried, and T. Schaetz, *Nature Communications* **7**, 11839 (2016).
- [24] See Supplemental Material for further details.
- [25] H. Kalis, *Initialization of Quantum States in a Two-Dimensional Ion-Trap Array*, Ph.D. thesis (2017).
- [26] A. Friedenauer, F. Markert, H. Schmitz, L. Petersen, S. Kahra, M. Herrmann, T. Udem, T. Hänsch, and T. Schätz, *Applied Physics B* **84**, 371 (2006).
- [27] M. Grifoni and P. Haenggi, *Physics Reports* **304**, 229 (1998).
- [28] Note: the phase relation of the ion oscillators results from different constant phase offsets, e.g. caused by supply

- wiring of the control electrodes, anharmonic contributions of the trapping potential or the duration between the start of excitation and modulation potentials.
- [29] D. A. Hite, Y. Colombe, A. C. Wilson, K. R. Brown, U. Warring, R. Jördens, J. D. Jost, K. S. McKay, D. P. Pappas, D. Leibfried, and D. J. Wineland, *Physical Review Letters* **109**, 103001 (2012).
 - [30] J. Labaziewicz, Y. Ge, P. Antohi, D. Leibbrandt, K. R. Brown, and I. L. Chuang, *Physical Review Letters* **100**, 013001 (2008).
 - [31] T. Schaetz, A. Friedenauer, H. Schmitz, L. Petersen, and S. Kahra, *Journal of Modern Optics* **54**, 2317 (2007).
 - [32] T. Schaetz, C. R. Monroe, and T. Esslinger, *New Journal of Physics* **15**, 085009 (2013).
 - [33] S. D. Huber and N. H. Lindner, *Proceedings of the National Academy of Sciences* **108**, 19925 (2011).
 - [34] A. Lemmer, C. Cormick, D. Tamascelli, T. Schaetz, S. F. Huelga, and M. B. Plenio, *New Journal of Physics* **20**, 073002 (2018).
 - [35] A. Bermudez, M. Bruderer, and M. B. Plenio, *Physical Review Letters* **111**, 040601 (2013).
 - [36] V. Peano, M. Houde, F. Marquardt, and A. A. Clerk, *Physical Review X* **6**, 041026 (2016).
 - [37] T. Ozawa, H. M. Price, A. Amo, N. Goldman, M. Hafezi, L. Lu, M. C. Rechtsman, D. Schuster, J. Simon, O. Zeitlinger, and I. Carusotto, *Reviews of Modern Physics* **91**, 015006 (2019).
 - [38] D. Porras and S. Fernández-Lorenzo, *Physical Review Letters* **122**, 143901 (2019).
 - [39] A. Bermudez and D. Porras, *New Journal of Physics* **17**, 103021 (2015).

Supplementary material: Floquet-engineered vibrational dynamics in a two-dimensional array of trapped ions

Philip Kiefer,^{1,*} Frederick Hakeberg,¹ Matthias Wittemer,¹
Alejandro Bermúdez,^{2,†} Diego Porras,^{3,‡} Ulrich Warring,¹ and Tobias Schaetz¹

¹*Albert-Ludwigs-Universität Freiburg, Physikalisches Institut,
Hermann-Herder-Strasse 3, 79104 Freiburg, Germany*

²*Departamento de Física Teórica, Universidad Complutense, 28040 Madrid, Spain*

³*Instituto de Física Fundamental IFF-CSIC,
Calle Serrano 113b, 28006 Madrid, Spain*

VIBRATIONAL DYNAMICS HAMILTONIAN

As proposed in [6, 7], a parametric modulation of the individual motional frequencies can induce effective vibrational dynamics described by the Hamiltonian

$$H = \sum_{\mathbf{j} > \mathbf{k}} \left(J_{\mathbf{j}\mathbf{k}}^{\text{eff}} e^{i\Phi_{\mathbf{j}\mathbf{k}}^{\text{P}}} a_{\mathbf{j}}^{\dagger} a_{\mathbf{k}} + \text{H.c.} \right) + \sum_{\mathbf{j}} V_{\mathbf{j}}(a_{\mathbf{j}}^{\dagger}, a_{\mathbf{j}}). \quad (1)$$

We have introduced bosonic operators that create-annihilate vibrational quanta (phonons) $a_{\mathbf{j}}^{\dagger}, a_{\mathbf{j}}$ at $T_{\mathbf{j}}$ of the 2D array. Hamiltonian (1) describes the vibrational dynamics in terms of the hopping of localized phonons between different ions. $J_{\mathbf{j}\mathbf{k}}^{\text{eff}}$ defines the Floquet-engineered tunneling strength, and $\Phi_{\mathbf{j}\mathbf{k}}^{\text{P}}$ is the so-called Peierls phase, which can mimic the coupling of a charged particle to an external electromagnetic field. We note that by modifying the strength of the parametric drive, we can tune $J_{\mathbf{j}\mathbf{k}}^{\text{eff}}$, while $\Phi_{\mathbf{j}\mathbf{k}}^{\text{P}}$ solely depends on the phases $\varphi_{\mathbf{j}}$ of the parametric drive of each individual trap. The exchange rate, which is directly accessible in the experiment, corresponds to $\Omega_{\text{AC}} = 2 \cdot J_{\mathbf{j}\mathbf{k}}^{\text{eff}}$. Finally, $V_{\mathbf{j}}(a_{\mathbf{j}}^{\dagger}, a_{\mathbf{j}})$ includes single-site terms, such as additional anharmonicities that can be interpreted as local phonon-phonon interactions.

PLANAR SURFACE-ELECTRODE TRAP ARRAY

We use a planar surface-electrode ion-trap array [1] with an electrode geometry optimized for isolation from the environment, inter-site coupling, and individual site control [2]. The trapping potential ϕ_{trap} is based on a global radio-frequency (rf) potential ϕ_{RF} and further tuned by local control potentials ϕ^{C} . Two rf electrodes are supplied in-phase with a zero-to-peak amplitude $U_{\text{RF}} \simeq 40$ V, oscillating at $\Omega_{\text{RF}}/(2\pi) \simeq 89$ MHz. Distinct control potentials ϕ^{C} are generated by 30 control electrodes, each connected to an arbitrary waveform generator with an output voltage of ± 10 V and an update rate of $2\pi \times 50$ MHz [3]. Initially, we evaporate Mg atoms below loading holes in the trap chip and photoionize near the $T_{\mathbf{j}}$. To fill the required trapping sites, we relocate ions between the $T_{\mathbf{j}}$ using dedicated control potentials. Each site can be loaded with single or multiple ions and we tune typical center of mass eigenfrequencies within the range of $2\pi \times (2 - 10)$ MHz.

EXPERIMENTAL REALIZATION OF THE PERIODIC MODULATION

In general, we could modulate the motional frequencies by periodically oscillating control curvatures [1]. Here, we realize the periodic modulation by exploitation of anharmonic third-order contributions of the trapping potential. Due to these anharmonic contributions, the motional eigenfrequencies depend on the position of the ion. By application of a control potential $\phi^{\mathcal{M}}$ with amplitude $u^{\mathcal{M}}$ the ion becomes displaced (up to $\simeq 1 \mu\text{m}$) and therefore its eigenfrequency changes. We characterize static effects of $\phi^{\mathcal{M}}$ on the lowest eigenfrequency $\omega_{\mathbf{j}}$ by

$$\omega_{\mathbf{j}}(u^{\mathcal{M}}) = c_{\mathbf{j}} + b_{\mathbf{j}} \cdot u^{\mathcal{M}} + a_{\mathbf{j}} \cdot (u^{\mathcal{M}})^2. \quad (2)$$

The harmonic contribution of the trapping potential is described by $c_{\mathbf{j}}$, higher third and fourth order contributions are characterized by $b_{\mathbf{j}}$ and $a_{\mathbf{j}}$, respectively.

Exemplary, we show measurement results for single ions in T_0 (blue) and T_1 (orange), and corresponding model fits in Fig. S1. To realize a near sinusoidal periodic modulation of the motional eigenfrequency, we require sufficient third order contributions $b_{\mathbf{j}}$. An oscillating control potential $\phi^{\mathcal{M}} \propto u^{\mathcal{M}} \cdot \sin(\Omega^{\mathcal{M}}t)$ leads in this case to a frequency modulation, with modulation index $\eta_{\mathbf{j}} = u^{\mathcal{M}} \cdot |b_{\mathbf{j}}|/\Omega^{\mathcal{M}}$ and modulation frequency $\Omega^{\mathcal{M}}$. Fourth order contributions of the local potentials $a_{\mathbf{j}}$ lead to an observable shift of the average eigenfrequency by $\delta_{\text{car},\mathbf{j}} \propto a_{\mathbf{j}}(u^{\mathcal{M}})^2$, while we can neglect effects on the modulation index $\eta_{\mathbf{j}}$. During all performed experimental sequences, we calibrate frequency shifts of $\omega_{\mathbf{j}}$ due to $\phi_{\mathbf{j}}^{\mathcal{M}}$, up to $|\delta_{\text{car},\mathbf{j}}|/(2\pi) \simeq 30 \text{ kHz}$. In general we can also modulate with a waveform that countervails the fourth order effects.

The modulation crosstalk between trapping sites depend on the static local potential at each site and the chosen modulation potential $\phi^{\mathcal{M}}$. To minimize crosstalk between the three sites, we modulate with $\phi_{\mathbf{j}}^{\mathcal{M}}$ applied up to three electrodes.

Model to derive modulation indices

In absence of the modulation, the frequency spectrum of the coherent motional excitation of an ion is described by the Fourier transform of the excitation pulse. Here the rectangular shaped excitation pulse leads to a *sinc*-shaped response of the ion [5]. The presence of the modulation causes characteristic sidebands. To determine the modulation indices $\eta_{\mathbf{j}}$ (see

Fig. 1) we model the motional excitation E of the ion with the function:

$$E(\eta_j) = \sum_{m=-\infty}^{\infty} \tilde{E}_j \cdot \mathcal{J}_m(\eta_j)^2 \cdot \text{sinc}(t^{\mathcal{M}}(\Omega^{\mathcal{E}} - (\tilde{\omega}_j + m \cdot \Omega^{\mathcal{M}} + \delta_{\text{car},j}))/2)^2 \quad (3)$$

where $\mathcal{J}_m(\eta_j)$ are Bessel functions of the first kind. The amplitude of the unmodulated coherent state is represented by \tilde{E}_j , the ion's unmodulated eigenfrequency by $\tilde{\omega}_j$ and the shift of the center frequency by $\delta_{\text{car},j}$. The modulation frequency is given by $\Omega^{\mathcal{M}}$, the excitation frequency by $\Omega^{\mathcal{E}}$. The simultaneous modulation and excitation is applied for a duration $t^{\mathcal{E}} = t^{\mathcal{M}}$.

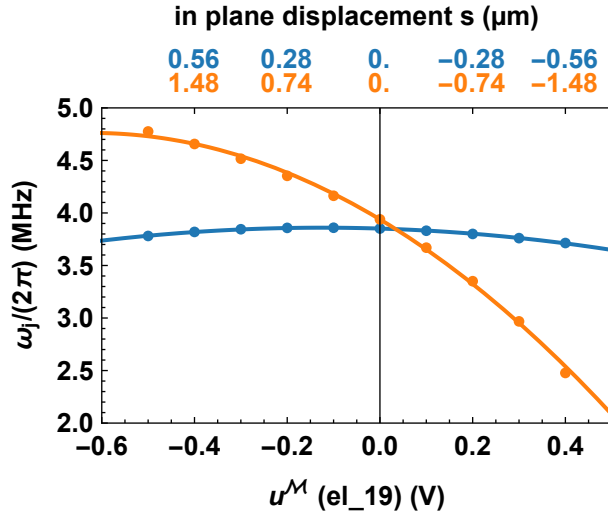


FIG. S1. **Characterization of anharmonic contributions of the trapping potential.** Static measured ω_j (ω_0 blue, ω_1 orange data points; errorbars are smaller than marker size) depending on the amplitude $u^{\mathcal{M}}$ of $\phi^{\mathcal{M}}$, generated by a single electrode ('el_19', see [4]). The solid lines represent model fits of equation (1), yielding $a_0/(2\pi) = -0.543(9)$ MHz/V², $b_0/(2\pi) = -0.135(3)$ MHz/V, $c_0/(2\pi) = 3.851(1)$ MHz, and $a_1/(2\pi) = -2.1(2)$ MHz/V², $b_1/(2\pi) = -2.65(4)$ MHz/V, $c_1/(2\pi) = 3.94(2)$ MHz/V². The crosstalk of the linear contribution at $u^{\mathcal{M}} = 0$ V is $b_0/b_1 = 5.1(1)\%$. The corresponding in-plane displacement at T_j is captured by a camera in a separate measurement. The top x-axis represent the ions' linear modeled displacements s parallel to the surface plane. Static out of plane mode orientations are typically below 25°, corresponding to a 10% enlarged displacement along its mode axis. We can rewrite the effect of the anharmonicities depending on the displacement s by $\omega_j(s)/(2\pi) = C_j + B_j \cdot s + A_j \cdot s^2$ with $A_0 = -0.280(7)$ MHz/(μm)², $B_0 = 0.097(2)$ MHz/(μm), $A_1 = -0.15(2)$ MHz/(μm)², $B_1 = 0.71(4)$ MHz/(μm) and $C_j = c_j$.

MODEL OF COHERENT PHONON EXCHANGE

We model the motional excitation \bar{n}_j of an initially Doppler cooled ion (with initial $\bar{n}_j < 20$) at T_j , which is coherently exchanging phonons with other sites by

$$\bar{n}_j(t_j^M) = N/2 \cdot (1 - \cos(\Omega_{AC} \cdot t_j^M) \cdot e^{-(t_j^M/\tau)^2}). \quad (4)$$

The exchange amplitude is given by N , and t_j^M describes the exchange duration. Instabilities of the eigenfrequencies, on timescales of ensemble averaging, are taken into account by a Gaussian dephasing term $e^{-(t_j^M/\tau)^2}$ with dephasing timescale τ . The initial contributions ($\bar{n}_j(t_j^M = 0) = 0$) are not considered for the model fits.

* philip.kiefer@physik.uni-freiburg.de; <https://www.qsim.uni-freiburg.de>

† albermud@fucm.es

‡ d.porras@iff.csic.es

- [1] M. Mielenz, H. Kalis, M. Wittemer, F. Hakelberg, U. Warring, R. Schmied, M. Blain, P. Maunz, D. L. Moehring, D. Leibfried, and T. Schaetz, *Nature Communications* **7**, 11839 (2016).
- [2] R. Schmied, J. H. Wesenberg, and D. Leibfried, *Physical Review Letters* **102**, 233002 (2009).
- [3] R. Bowler, U. Warring, J. W. Britton, B. C. Sawyer, and J. Amini, *Review of Scientific Instruments* **84**, 033108 (2013).
- [4] H. Kalis, F. Hakelberg, M. Wittemer, M. Mielenz, U. Warring, and T. Schaetz, *Physical Review A* **94**, 023401 (2016).
- [5] H. Kalis, *Initialization of Quantum States in a Two-Dimensional Ion-Trap Array*, Ph.D. thesis (2017).
- [6] A. Bermudez, T. Schaetz, and D. Porras, *Physical Review Letters* **107**, 150501 (2011).
- [7] A. Bermudez, T. Schaetz, and D. Porras, *New Journal of Physics* **14**, 053049 (2012).